Multiscale Phase Mapping of $LiFePO_4$-Based Electrodes by Transmission Electron Microscopy and Electron Forward Scattering Diffraction

Donatien Robert,[†] Thierry Douillard,[§] Adrien Boulineau,[†] Guillaume Brunetti,[⊥,#] Pawel Nowakowski,[∥] Denis Venet,[†] Pascale Bayle-Guillemaud,[‡] and Cyril Cayron[†,*]

[†]CEA, DRT, LITEN, DEHT, Minatec, 17 Rue des Martyrs, 38054 Grenoble, France, [‡]CEA, DSM, INAC/UJF, LEMMA, Minatec, 17 Rue des Martyrs, 38054 Grenoble, France, [§]INSA-Lyon, MATEIS, 7 Avenue Jean Capelle, 69621 Villeurbanne, France, [⊥]CEA, LETI, DTSI, SCMC, Minatec, 17 Rue des Martyrs, 38054 Grenoble, France, and [∥]Oxford Instruments, 91400 Gometz la Ville, France. [#]Present address: JEOL France 78290 Croissy sur Seine, France.

ABSTRACT $LiFePO_4$ and $FePO_4$ phase distributions of entire cross-sectioned electrodes with various Li content are investigated from nanoscale to mesoscale, by transmission electron microscopy and by the new electron forward scattering diffraction technique. The distributions of the fully delithiated ($FePO_4$) or lithiated particles ($LiFePO_4$) are mapped on large fields of view (>100 × 100 μm^2). Heterogeneities in thin and thick electrodes are highlighted at different scales. At the nanoscale, the statistical analysis of 64 000 particles unambiguously shows that the small particles delithiate first. At the mesoscale, the phase maps reveal a core–shell mechanism at the scale of the agglomerates with a preferential pathway along the electrode porosities. At larger scale, lithiation occurs in thick electrodes "stratum by stratum" from the surface in contact with electrolyte toward the current collector.

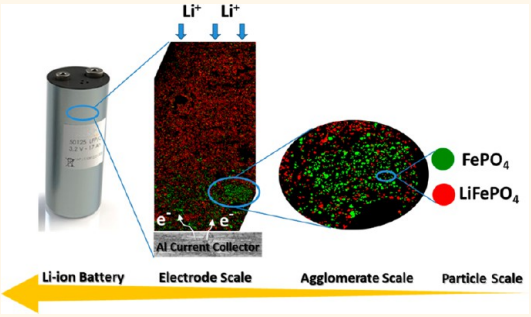

KEYWORDS: $LiFePO_4$ · LFP · electron microscopy · EFSD · t-EBSD · TKD · phase mapping · heterogeneities

Since the pioneering work of Padhi *et al.*[1] in 1997, many investigations on Li_xFePO_4 (with $0 \leq x \leq 1$) have been performed. The material has a theoretical capacity of 170 mAh/g and undergoes at room temperature a first-order transition at 3.45 V *vs* Li^+/Li between a Li-rich phase and a Li-poor phase[2] called in this paper LFP and FP, respectively. To overcome a relative low capacity, the electrodes need to be highly loaded in active material by using thick electrodes (>100 μm), leading to a capacity loss during cycling that becomes an important issue.[3] The understanding of the fading mechanisms in thick electrodes is then essential for improving the performances of the batteries using LFP as cathode material. The aim of this paper is to give a wider view on the lithiation mechanisms occurring in thin and thick LFP/FP electrodes at different scales. The term "nanoscale" refers to phenomena at the particle scale, and the term "mesoscale" refers to the cluster scale relative to assemblies of tens to hundreds of particles. Larger scales correspond to the whole electrode thickness.

So far, at the nanoscale, several two-phase reaction models have been proposed: the shrinking core–shell model,[1,4] the spinodal-decomposition model,[5] the radial core–shell model,[6] and the domino-cascade model.[7,8] They were generally deduced from transmission electron microscopy (TEM) investigations[6−11] and related techniques such as electron energy loss spectroscopy (EELS),[6] energy filtered transmission electron microscopy (EFTEM),[11] and precession electron diffraction (PED).[8] The domino-cascade model stipulates that the small particles are found either fully lithiated (LFP) or fully delithiated (FP) during the charge/discharge of the battery due to a very rapid lithiation/delithiation front. The domino-cascade model was experimentally confirmed in the equilibrium state after partial delithiation.[8] Theoretical studies also played a significant role for a better

* Address correspondence to cyril.cayron@cea.fr.

Received for review August 22, 2013 and accepted November 5, 2013.

Published online November 05, 2013
10.1021/nn4043964

understanding of the mechanisms. For example, *ab initio* calculations have shown that the easy diffusion paths of lithium ions are tunnels parallel to the direction *b*.[12,13] Ceder's group[14] calculated the shape of the free energy curve of a single particle and showed that a solid-solution could exist in nonequilibrium conditions, leading to either fully lithiated or delithiated particles after relaxation when the particles are small. Indeed, the final relaxed state of the particles depends on the particle size, as described by Wagemaker *et al.*[15] The many-particle model of Dreyer *et al.*[16] proposes that the particles reach the fully lithiated or fully delithiated equilibrium state during the relaxation by interchange of lithium thought interparticle pathways. Sasaki *et al.*[17] recently evidenced a memory effect in $LiFePO_4$ electrodes and used the many-particle model to explain it.

At the mesoscale, in the case of the small particles, Delmas *et al.*[7] suggested in their discussion that (de)lithiation could occur, particle by particle, at the surface of dense agglomerates. This core−shell mechanism would occur at the agglomerate scale, which seems in agreement with the PED and EFTEM images obtained in our previous work,[8] but the number of analyzed particles was not sufficient at that time for an unambiguous experimental confirmation. Despite these works, a "mosaic" model describing a homogeneous mixture of particles, either LFP particles or FP particles, in the entire electrode is generally assumed.[16,18] Very recently, a scanning transmission X-ray microscopy (STXM)[19] analysis of 450 particles with a spatial resolution of 40 nm was shown to be consistent with this homogeneous phase distribution through the thickness of an LFP-based electrode.

At larger scales, typically some hundreds of micrometers, other characterization techniques such as nuclear magnetic resonance (NMR),[20] X-ray, or neutron diffraction[2,7,21,22] and X-ray photoelectron spectroscopy (XPS)[23,24] give average information on the nature and ratios of phases in the electrodes. X-ray microdiffraction[25] was employed for phase mapping with a resolution of several micrometers. Recently, Ouvrard *et al.*[26] highlighted some heterogeneities and delay in the lithiation process by using *in operando* X-ray absorption spectroscopy (XAS). However, the design of the special electrochemical cell, particularly the low electrical contact in the region of analysis, could explain these phenomena.

Despite all these investigations and progresses in the understanding of the lithiation mechanisms, some questions still remain. Is the (de)lithiation homogeneous or heterogeneous for a large amount of particles along the electrode thickness? Two scenarios of phase distribution seem compatible with the models detailed in the previous section and with the electrochemical studies.[27,28] Let us give an example with an 80% lithiated electrode, as presented in Figure 1. In the first scenario, the intercalation would begin particle by particle globally everywhere over the whole thickness of the electrode (no preferential pathway), creating an unstable new phase, Li_xFePO_4 (with $x \approx 0.6$).[29] The relaxation of the battery would yield a random distribution along the thickness. In the second scenario, the intercalation would occur "stratum by stratum" from the surface in contact with the electrolyte to the current collector following a fast phase reaction front between the coming Li ions and the particles. After relaxation, the electrode would form a phase gradient along the thickness with much more lithiated particles at the surface side compared to the collector side. This work presents maps of FP and LFP phases that give a global view of the intercalation/deintercalation mechanism in LFP-cathodes at different scales and determine the final phase distribution at the thermodynamic equilibrium. The distributions of the FP and LFP phases inside thin and thick electrodes of different types of lithium batteries are studied.

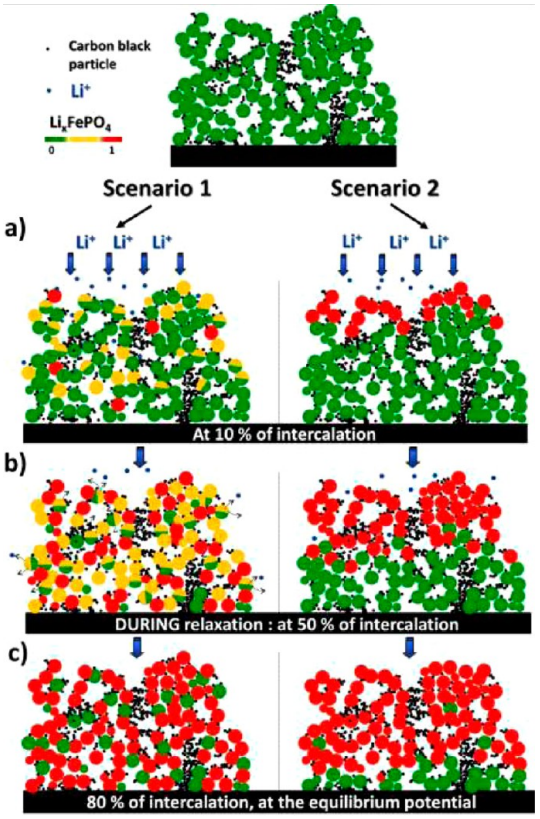

Figure 1. Two possible scenarios of the intercalation mechanism across the electrode thickness at different steps of lithiation. (a) Dynamically at 10% lithiation (before relaxation). Scenario 1: The intercalation forms a solid solution in the electrode. Scenario 2: The intercalation begins at the top of the electrode. (b) During the battery relaxation at 50% lithiation. Scenario 1: The solid solution particles in an unstable state become either fully lithiated or fully delithiated by local lithium interchange in a random way. Scenario 2: The particles are in a stable state. (c) At 80% of lithiation. Scenario 1: The LFP/FP phase distribution is random in the whole electrode. Scenario 2: Only the top of the electrode is lithiated "stratum by stratum" from the surface to the current collector.

RESULTS AND DISCUSSION

Since 2011, we have improved the PED and EFTEM techniques in terms of resolution and sensitivity; the quality of the PED and EFTEM phase maps shown in Figure S1 now allows us to confirm the fully lithiated and delithiated state of the particles in lithiation, completing the work done in delithiation.[8] Nevertheless, these TEM techniques provide only nanoscale mapping due to a field of view limited to a few μm^2, typically 5 μm × 5 μm. To complete them, a very new technique called electron forward scattering diffraction (EFSD) working in a scanning electron microscope (SEM) is employed on cycled electrodes in order to get phase maps on much larger fields of view (>100 μm × 100 μm), *i.e.*, more than the entire electrode thickness, while maintaining a nanometric resolution. Like PED, EFSD is also based on diffraction. The TEM thin lamella prepared by ultramicrotomy is mounted into the SEM close to the pole piece, a standard electron backscatter diffraction (EBSD) camera is inserted below the sample, and the Kikuchi patterns are acquired and treated almost as in an EBSD experiment. Since the EFSD technique is very new, its name is not yet definitively chosen in the scientific community; other names such as t-EBSD (t for transmission) or transmission Kikuchi diffraction (TKD) are also given.[30−32] Despite the small difference of lattice parameters of the FP and LFP phases (<5%), EFSD, like PED, is able to discriminate between the two phases, as proved by our tests on pure powders: Figure S2 shows experimental results obtained on the pristine LFP electrode, on the chemically delithiated powder (Figures S3 and S4), and on the electrochemically delithiated FP electrode (Figure S5), with indexation rates higher than 85%.

Thin Electrodes after Partial Delithiation. For the investigations across the thickness of thin electrodes in cycled coin cells, the cycling was stopped after six and a half charges (50% of theoretical delithiation), as shown in Figure S6. An ultramicrotomy-prepared cross section was extracted from the center of the electrode. Three PED phase maps (1 × 1 μm) at a distance of approximately 2, 7, and 12 μm from the electrode surface are shown in Figure 2. The spatial resolution of these maps is 10 nm (step between two diffraction patterns). It is shown that the particles after the partial charge are either fully lithiated (in red) or fully delithiated (in green), in agreement with our previous work.[8] The FP ratios are 26.7%, 15.1%, and 23.6% for maps 1, 2, and 3, respectively. The average FP content is 22%, which is lower than the expected 50%: the FP phase is underrepresented in the center of the electrode. Moreover, no gradient along the thickness of the electrode could be evidenced, indicating that the diffusion of electrolyte and electron transport are not the limiting factors. However, the limited field of view can hide some larger scale phenomena. In order to increase the field of view

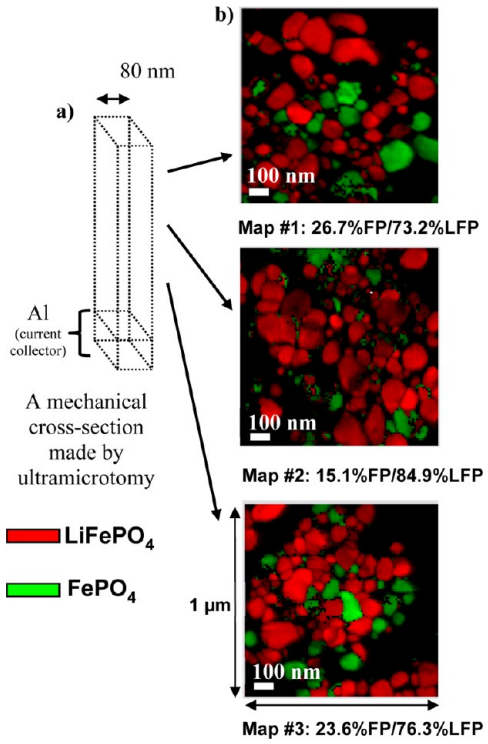

Figure 2. (a) Schematic view of a cross-section of the LFP-based electrode after a cycling of seven and a half charges and analysis along its ~80 nm thickness. (b) PED phase maps at 2, 7, and 12 μm from the surface. The green and red phases represent FP and LFP phases, respectively.

while maintaining a high spatial resolution, EFSD characterizations have been performed on the same area. The SEM image and the EFSD phase map obtained on the entire electrode are shown in Figure 3a and b, respectively. Both LFP and FP phases are present. The particles are monocrystalline and monophasic, and no LFP/FP gradient along the thickness is observed. The area marked 1 reveals a global heterogeneous mix with a composition of 33% FP phase, confirming the underrepresentation of the FP phase. Moreover, other areas on the map exhibit large lithiated or delithiated zones, revealing heterogeneities at larger scale. The quantification of the circled areas marked 2 to 5 in the EFSD phase map of Figure 3b shows agglomerates mainly composed of single phase particles (LFP or FP), with LFP/FP ratios presented in Figure 3e. These agglomerates are distributed over the whole thickness with sizes ranging between 2 and 10 μm^2. This could explain the differences of phase ratios measured on the small localized area imaged by PED in Figure 2.

Other ultramicrotomy-prepared cross sections were extracted from the edge of the same electrode and investigated by EFSD. A typical map is presented in Figure 3d, and more maps acquired on the same cross-section sample are reported in Figure S7. They show that the FP phase (84% in average) is now overrepresented at the edge of the electrode. Moreover, the FP agglomerates now spread over several hundred

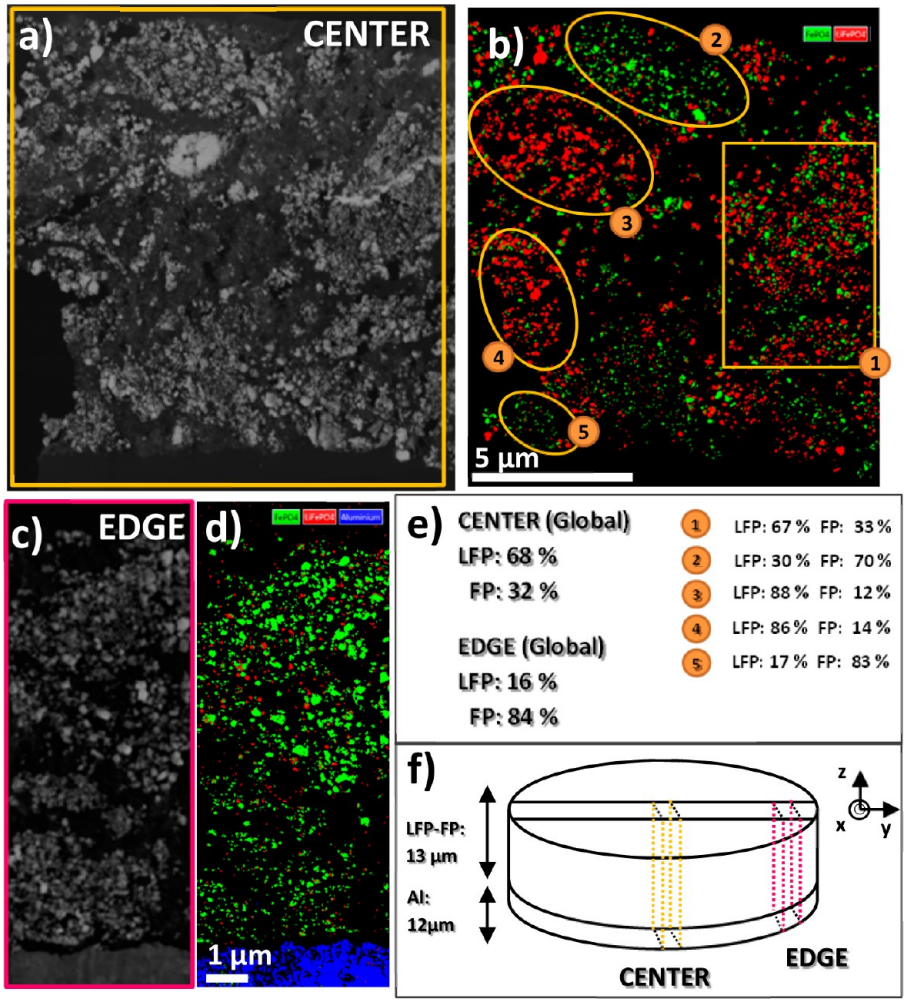

Figure 3. (a) SEM image of the cross section of a thin electrode after seven and a half charges (stopped at 50% of theoretical delithiation) extracted from the center of the electrode. (b) Corresponding EFSD phase map. Agglomerates of LFP or FP particles are clearly visible: some are marked by ellipses. (c) SEM image and (d) EFSD phase map of another sample extracted from the edge of the same electrode. (e) Global LFP/FP quantification of the two samples extracted from the center and edge, and local quantification of the phase map (b). (f) Global schematic view of the electrode indicating the localization of the two regions. The diameter of the electrode is 14 mm.

micrometers to probably a few millimeters. The XRD analysis shows a global composition (center and edge) of 64% of FP phase, as shown in Figure S8, which is indeed between the 33% FP found in the center and the 84% FP found at the edge. These results are consistent with *in situ* XRD[33,34] and with the recent *in operando* XAS study of Ouvrard *et al.*,[26] who observed that some parts of the electrode are delayed and others are advanced with regard to the mean charge state of the electrode. EFSD clearly reveals that the lithiation/delithiation mechanism taking place across the electrode is heterogeneous and leads to micrometric FP or LFP phase-rich agglomerates with larger agglomerates at the edge of the electrode.

Thick Electrodes after Partial Delithiation. The thick electrode (130 μm) was stopped during the first charge at 20% theoretical delithiation in a Li//$LiFePO_4$ coin cell. Some EFSD phase maps obtained with a step size of 40 nm are presented in Figure 4. The large map of Figure 4c was sliced into 10 parts from the surface toward the current collector, and the evolution of the FP/LFP phase ratio through each slice is presented in Figure 4d. A phase gradient along the electrode thickness is visible. Slice no. 1 close to the surface contains 28% FP phase, whereas on the other side close to the collector slice no. 10 contains 16% FP phase. The XRD quantification performed on both sides of the electrodes confirms the phase contents, as presented in Figures S9 and S10.

An EFSD map was acquired close to the surface at higher magnification (Figure 4b). The blue frontiers delimit the remaining LFP dense agglomerates surrounded by FP particles. The white arrows highlight the lithium pathway during the delithiation. Figure S11 confirms in detail the phase map for the extreme slices 1 and 10 and emphasizes the phenomenon. It can be noticed that dense agglomerates of LFP particles (in red) are surrounded by FP particles (in green).

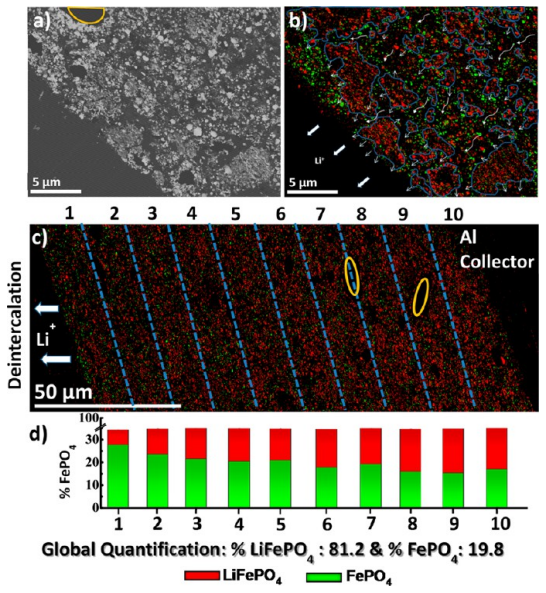

Figure 4. (a) SEM image of the thick electrode (130 μm) stopped at 20% theoretical delithiation during the first charge. (b) EFSD phase map on the same area. The blue frontiers delimitate LFP dense agglomerates surrounded by FP particles. The white arrows highlight the lithium pathway. (c) EFSD phase map on the whole electrode thickness. The map is segmented into 10 parts. (d) Phase quantification of the different parts from the surface in contact with the electrolyte (no. 1) to the current collector (no. 10). An FP gradient is visible. The orange ellipses show voids created during the sample preparation by ultramicrotomy.

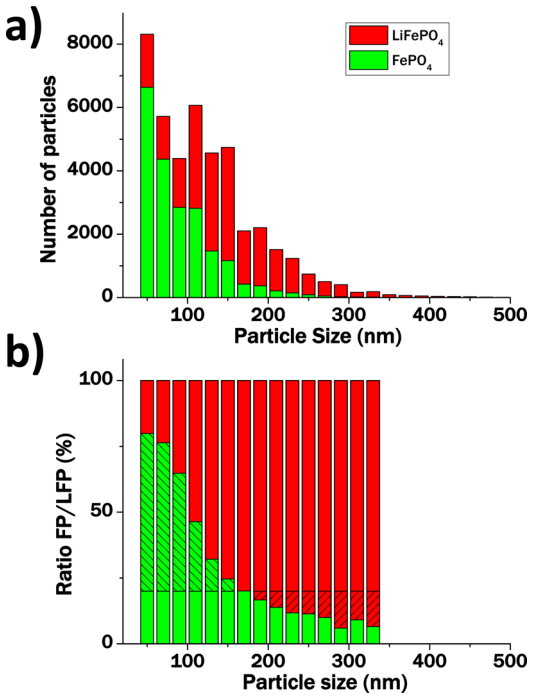

Figure 5. (a) Particle size distribution for the phase map of Figure 4a corresponding to 20% of the first delithiation in the thick electrode (130 μm). (b) FP/LFP ratio function of the particle sizes. The ratio was calculated for a number of particles higher than 100 (which explains that there is no bar for particles larger than 340 nm). The line at 20% represents the average ratio between FP/LFP if the delithiation was equiprobable. The hatched part shows the deviation from this value (over- or under-representation of the FP phase).

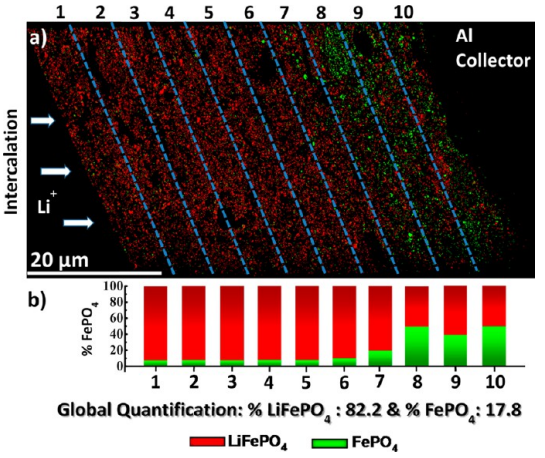

Figure 6. (a) EFSD phase map of a thick electrode (55 μm) extracted from the Li ion cell stopped after 45 cycles and fully discharged. The electrode is expected to be completely LFP, but in (b) the map shows clearly the presence of the FP region close to the collector. LFP and FP particles are represented in red and green color, respectively.

A careful examination shows that delithiation seems to begin from the continuous paths of porosity. A core–shell mechanism at agglomerate scale seems to take place; the delithiation would begin near the surface in contact with the electrolyte and propagates across the thickness of the electrode by continuous pathways of higher porosity, leaving agglomerates of lithiated particles (in red) surrounded by shells of delithiated particles (in green), like isolated islands surrounded by rivers. A core–shell deintercalation mechanism at the agglomerate scale is consistent with Srinivasan *et al.*'s simulations[35] and Delmas's supposition.[7]

More than 64 000 particles are indexed in the map of Figure 4a; their diameters were calculated using the square root of the particle area, and the size distribution is given in Figure 5a. The FP/LFP ratios as functions of the sizes are presented in Figure 5b. The hatched part marks the FP over-represented (above the line) or under-represented (under the line) compared to the expected average 20% value. The particles under 50 nm could not be statistically counted due to the step size used for the map acquisition (40 nm). Contrary to what we thought from our previous work,[8] this histogram clearly highlights that the smaller particles were the first to delithiate. These results are consistent with Delmas *et al.*'s expectations.[7]

Thick Electrodes after Lithiation. The lithium ion cell was cycled 45 times at C/3 rate (1 mol of lithium per 3 h) after a C/20 rate formation cycling. An EFSD phase map on the fully discharged electrode is presented in Figure 6a. The map should be totally red (fully LFP); however an important presence of FP particles localized close to the current collector is clearly visible. The local quantification (Figure 6b) shows that the three slices close to

the current collector contain more than 40% FP phase, whereas on the other side the other slices close to the surface contain only 8% FP phase on average. This macroscopic heterogeneity was confirmed by global XRD analyses acquired on the surface side (2% FP) and on the current collector side (48% FP), as shown in Figures S12 and S13. The analysis depth according to the LFP density and electrode porosity (around 40%) is estimated by the Absorb DR software at 4 and 26 μm for $2\vartheta = 10°$ and 80°, respectively. The presence of the retained FP phase close to the collector can be explained by the loss of lithium due to its trapping in the solid electrolyte interface[36] essentially on the graphite anode,[37−40] in agreement with the 14% capacity loss after the first cycle and the 8% added after 45 cycles measured on the electrochemical curve reported in Figure S14. The ESFD map shows that the lithiation starts from the particles at the surface in direct contact with the electrolyte and propagates "stratum by stratum". A nonuniform phase distribution during the lithiation at high current density (18 C) was already observed by Liu *et al.*[25] using synchrotron microdiffraction for an LFP-based electrode with a thickness of ~50 μm. However they found a uniform distribution for a low rate (C/9), whereas a strong gradient phase distribution is observed in our electrode. These results are also consistent with the XPS surface analysis performed by Castro *et al.*[24] revealing a higher Fe^{2+}/Fe^{3+} ratio between the surface side and the collector side. This phase map highlights that the electronic diffusion is not the limiting factor, but the reaction is controlled by Li^+ ion diffusion across the thick electrode. Fongy *et al.*[41] discussed this point by varying the porosity and thickness parameters in the calculations. An investigation of the negative electrode could clarify the aging mechanisms of the graphite//$LiFePO_4$ batteries.

All the characterizations were performed *ex situ* and do not contain any kinetic information. So the present experimental results cannot be used to unambiguously determine whether there is a metastable solid solution phase formed dynamically or a fast complete reaction at the scale of the particle, as proposed in the domino-cascade model. However, these results seem in fair agreement with scenario 2 of Figure 1. At least, the large heterogeneities prove that if an intermediate fleeting solid solution phase was formed in all the particles during the lithiation, the relaxation into fully lithiated and delithiated phases could not occur between neighboring particles as proposed in the literature, but should occur by agglomerates.

Effects of Defects on Lithiation/Delithiation Reaction. All the PED and ESFD maps confirm that the majority of particles are either fully lithiated or fully delithiated. However, some mixed particles can be observed occasionally (1%). One case was studied in a half-charged LFP-based electrode by PED and EFTEM (Figure 7a and c). The particle marked by an orange square

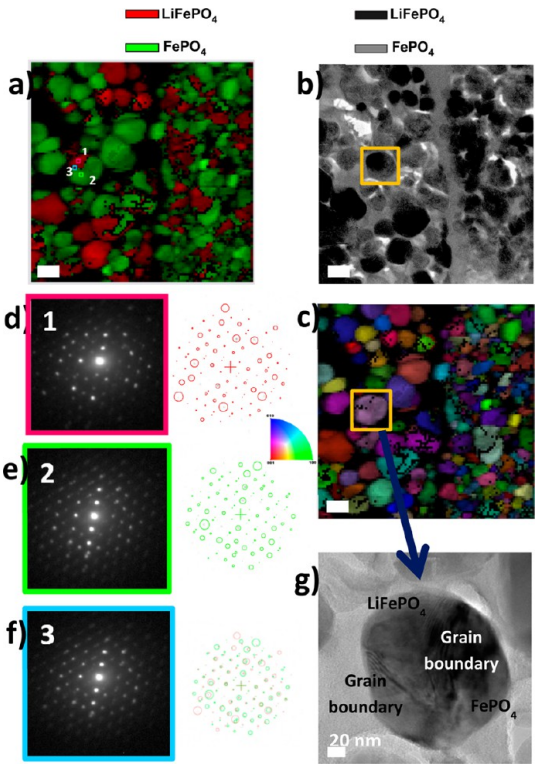

Figure 7. Phase maps on an electrode stopped at half-charge. (a) PED phase map. (b) EFTEM phase map obtained by a ratio of two filtered images centered at 5 and 25 eV on the same region. (c) Orientation map deduced from map a. The inverse pole figure color coding is given next to the map. (d, e, and f) Experimental PED patterns extracted from the rose, green, and blue squares on phase map a (at the left) and the LFP and FP theoretical templates, in red and green, respectively (at the right). (g) TEM image of a particle (marked in c by the orange square) presenting a subgrain boundary that stopped the delithiation process. The diffraction in f acquired at this subgrain boundary results from the superposition of the FP and LFP phases. The scale bar in a, b, and c is 100 nm.

contains the two LFP/FP phases. The orientation map in Figure 7c shows that the two parts of the biphasic particle have nearly the same orientation. The experimental and simulated diffraction patterns extracted from areas 1 and 2 are presented in Figure 7d and e. The interphase boundary marked 3 appears with black pixels because of the low reliability indexes (Figure 7f). No solid-solution could be revealed at the interphase, in good agreement with Laffont's study.[6] The contrast in the TEM image of the interphase (Figure 7g) is typical of a subgrain boundary (<5°). According to the domino-cascade model, if the elastic wave propagating in the *a* direction meets some defects during the intercalation/deintercalation reaction, the reaction front is interrupted,[7] in good agreement with our observation. This highlights that some rare biphasic particles containing defects can be detected, and this does not contradict the domino-cascade model.

CONCLUSION

In summary, a combination of several techniques has been used to perform FP/LFP phase mapping on

thin (13 μm) and thick (55 and 130 μm) LFP-based electrodes, at the nanoscale by PED and EFTEM, and for the first time at the mesoscale by EFSD. EFSD is a powerful technique with a spatial resolution better than 10 nm and field of view larger than 100 μm $\times$ 100 μm, which perfectly fills the requirements for FP/LFP mapping of semi-industrial thick electrodes. At the nanoscale, the fully lithiated and delithiated state of the particles in equilibrium state, previously confirmed for delithiation, is now experimentally confirmed for lithiation. The rare biphasic particles (<1%) could be attributed to subgrain boundaries in the pristine particles. In thin electrodes the average lithium content does not vary across the thickness, but some rich FP or LFP agglomerates of particles have been observed. In thick electrodes, the EFSD maps show two types of phase gradient across the electrode thickness: at the mesoscale, (de)lithiation was shown to occur by an "agglomerate core−shell" mechanism and, at larger scale, by a "stratum by stratum" mechanism. These heterogeneities can probably be explained by the local equilibrium of lithium in the electrolyte. Close to the electrode surface, there is nearly no lithium saturation in the electrolyte and the lithium exchange with particles is not limited. The particles that (de)lithiate first are those at the surface in direct contact with the electrolyte. Far from the surface, the lithium concentration is probably saturated in the porosities. Lithium follows preferential pathways along the percolations of large porosities, leaving isolated agglomerates. The ionic diffusion is the main limiting factor at the origin of the two heterogeneities. After cycling and capacity fading, some lithium is lost probably in the graphite anode, and the particles of the LFP electrode close to the current collector become "inactive". Finally, EFSD opens new perspectives for the multiscale studies of the lithiation mechanisms in LFP/FP and other Li-ion crystalline materials.

METHODS

Electrode Processing. Thin electrodes (13 μm) were prepared from a 500 mg mixture of 80 wt % $LiFePO_4$ active material with 10 wt % Super P carbon black (Timcal) and 10 wt % poly(vinylidene difluoride) binder (Solef 1015, Solvay) in *N*-methylpyrrolidone. This mixture was then cast onto an aluminum foil by doctor blade and dried overnight at 55 °C. The electrodes were weighed with 5 mg of active material. Thick electrodes (130 μm) were coated on a Coatema machine with a loading of 4.5 mAh/cm^2 from a mixture with a close composition of thin electrodes. Discs 14 mm in diameter were finally punched for the thin and thick electrodes, pressed at 6.5 T/cm^2, and dried for 48 h at 80 °C under vacuum. The negative electrode is a disk of lithium metal foil. Two separators in polypropylene wetted by the liquid electrolyte in a mixture of propylene carbonate/ethylene carbonate/dimethyl carbonate (1:1:3) containing $LiPF_6$ as salt (1 mol·L^{-1}) were placed between the two electrodes. These lithium metal cells were assembled in a drybox under argon. A stable capacity was obtained after two cycles. The electrochemical cell was cycled with a C/20 rate. The lithium ion cell (17 Ah) consists of a LFP-based electrode (thickness of 55 μm) and graphite as counter electrode. The porosity and the loading of the LFP-based electrode were evaluated at 40% and 3 mAh, respectively. The polypropylene separator is soaked in the liquid electrolyte composed of a mixture of carbonate containing some additives and $LiPF_6$ as salt (1 mol·L^{-1}). The formation of the cell was performed at C/20 for the first cycle, and then it cycled at C/3. After relaxation (12 h), the electrodes were disassembled in the glovebox, washed in dimethyl carbonate, and dried under argon.

Materials Characterization. The electrodes were mechanically cross-sectioned by ultramicrotomy to obtain samples thin enough for the TEM and EFSD analyses (~80 nm) and avoid overlapping of particles. The size of the LFP particles used in this study ranges between 50 and 300 nm. PED maps were acquired on a Jeol 2010 FEF working at 200 kV with the ASTAR system. An external "fast optical" CCD camera (AVT Stingray) was used for the acquisition of the PED patterns. They were recorded as 256 $\times$ 256 pixel images with an 8-bit dynamical range. The external position of the camera introduces some distortions in the diffraction patterns, which are corrected during the data treatment. The camera length and the distortions are calculated using a silicon sample oriented along the [110] direction as the reference sample. These parameters were kept constant for the treatment of maps acquired during the same session (typically for a day). The PED patterns were obtained with a 10 μm condenser aperture, a convergence angle of 0.6 mrad, a camera length of 60 cm, and a spot size (diameter) of 2.6 nm (full width at half-maximum) without precession and 2.7 nm with a precession angle of 0.96°. EFTEM was performed at 200 kV on the same microscope equipped with a Tridiem Gatan imaging filter. A series of EFTEM images with an energy selecting slit of 1 eV were acquired to fill the so-called data cube (x,y,ΔE), ΔE being the electron energy loss and x and y denoting the position in the image. The EELS spectra were reconstructed from these stacks of EFTEM images using Digital Micrograph module "Spectrum Imaging". EFSD maps were all acquired on a Zeiss Supra 55 VP SEM working in high current mode with an acceleration voltage of 30 kV and an aperture of 60 μm. The Oxford Instruments Nordlys S EBSD detector coupled with an AZtec system was employed for EFSD analyses.

Conflict of Interest: The authors declare no competing financial interest.

Acknowledgment. The authors wish to thank S. Ubhi (Oxford Instruments), who drew our attention to the new EFSD technique, T. Gutel for the chemical delithiation, S. Genies, L. Daniel, F. Dewulf, N. Martin, C. Barchasz, J. F. Martin, S. Patoux, and S. Martinet for the electrochemical discussions, and J. F. Colin for his piece of advice about XDR. This study was partially funded thanks to the French ANR project AMOS and to the Carnot project Vehy-Loco.

Supporting Information Available: Details of the preparation of the reference materials, validation of the EFSD technique on pure materials, high-resolution EFSD phase maps, XRD analysis with Rietveld refinement, and charge/discharge voltage profiles are provided. This material is available free of charge *via* the Internet at http://pubs.acs.org.

REFERENCES AND NOTES

1. Padhi, A. K.; Nanjundaswamy, K. S.; Goodenough, J. B. Phospho-Olivines as Positive-Electrode Materials for Rechargeable Lithium Batteries. *J. Electrochem. Soc.* **1997**, *144*, 1188–1194.
2. Yamada, A.; Koizumi, H.; Nishimura, S.; Sonoyama, N.; Kanno, R.; Yonemura, M.; Nakamura, T.; Kobayashi, Y. Room-Temperature Miscibility Gap in Li_xFePO_4. *Nat. Mater.* **2006**, *5*, 357–360.

3. Yu, D. Y. W.; Donoue, K.; Inoue, T.; Fujimoto, M.; Fujitani, S. Effect of Electrode Parameters on $LiFePO_4$ Cathodes. *J. Electrochem. Soc.* **2006**, *153*, A835–A839.
4. Srinivasan, V.; Newman, J. Discharge Model for the Lithium Iron-Phosphate Electrode. *J. Electrochem. Soc.* **2004**, *151*, A1517–A1529.
5. Ramana, C. V.; Mauger, A.; Gendron, F.; Julien, C. M.; Zaghib, K. Study of the Li-Insertion/Extraction Process in $LiFePO_4$/$FePO_4$. *J. Power Sources* **2009**, *187*, 555–564.
6. Laffont, L.; Delacourt, C.; Gibot, P.; Wu, M. Y.; Kooyman, P.; Masquelier, C.; Tarascon, J. M. Study of the $LiFePO_4$/$FePO_4$ Two-Phase System by High-Resolution Electron Energy Loss Spectroscopy. *Chem. Mater.* **2006**, *18*, 5520–5529.
7. Delmas, C.; Maccario, M.; Croguennec, L.; Le Cras, F.; Weill, F. Lithium Deintercalation in $LiFePO_4$ Nanoparticles *via* a Domino-Cascade Model. *Nat. Mater.* **2008**, *7*, 665–671.
8. Brunetti, G.; Robert, D.; Bayle-Guillemaud, P.; Rouvière, J. L.; Rauch, E. F.; Martin, J. F.; Colin, J. F.; Bertin, F.; Cayron, C. Confirmation of the Domino-Cascade Model by $LiFePO_4$/$FePO_4$ Precession Electron Diffraction. *Chem. Mater.* **2011**, *23*, 4515–4524.
9. Chen, G.; Song, X.; Richardson, T. J. Electron Microscopy Study of the $LiFePO_4$ to $FePO_4$ Phase Transition. *Electrochem. Solid-State Lett.* **2006**, *9*, A295–A298.
10. Gu, L.; Zhu, C.; Li, H.; Yu, Y.; Li, C.; Tsukimoto, S.; Maier, J.; Ikuhara, Y. Direct Observation of Lithium Staging in Partially Delithiated $LiFePO_4$ at Atomic Resolution. *J. Am. Chem. Soc.* **2011**, *133*, 4661–4663.
11. Moreau, P.; Mauchamp, V.; Pailloux, F.; Boucher, F. Fast Determination of Phases in Li_xFePO_4 Using Low Losses in Electron Energy-Loss Spectroscopy. *Appl. Phys. Lett.* **2009**, *94*, 123111–3.
12. Morgan, D.; Van der Ven, A.; Ceder, G. Li Conductivity in Li_xMPO_4 (M = Mn, Fe, Co, Ni) Olivine Materials. *Electrochem. Solid-State Lett.* **2004**, *7*, A30–A32.
13. Islam, M. S.; Driscoll, D. J.; Fisher, C. A. J.; Slater, P. R. Atomic-Scale Investigation of Defects, Dopants, and Lithium Transport in the $LiFePO_4$ Olivine-Type Battery Material. *Chem. Mater.* **2005**, *17*, 5085–5092.
14. Malik, R.; Zhou, F.; Ceder, G. Kinetics of Non-Equilibrium Lithium Incorporation in $LiFePO_4$. *Nat. Mater.* **2011**, *10*, 587–590.
15. Wagemaker, M.; Mulder, F. M.; Van der Ven, A. The Role of Surface and Interface Energy on Phase Stability of Nanosized Insertion Compounds. *Adv. Mater.* **2009**, *21*, 2703–2709.
16. Dreyer, W.; Jamnik, J.; Guhlke, C.; Huth, R.; Moškon, J.; Gaberšček, M. The Thermodynamic Origin of Hysteresis in Insertion Batteries. *Nat. Mater.* **2010**, *9*, 448–453.
17. Sasaki, T.; Ukyo, Y.; Novák, P. Memory Effect in a Lithium-Ion Battery. *Nat. Mater.* **2013**, *12*, 569–575.
18. Van der Ven, A.; Garikipati, K.; Kim, S.; Wagemaker, M. The Role of Coherency Strains on Phase Stability in Li_xFePO_4: Needle Crystallites Minimize Coherency Strain and Overpotential. *J. Electrochem. Soc.* **2009**, *156*, A949–A957.
19. Chueh, W. C.; El Gabaly, F.; Sugar, J. D.; Bartelt, N. C.; McDaniel, A. H.; Fenton, K. R.; Zavadil, K. R.; Tyliszczak, T.; Lai, W.; McCarty, K. F. Intercalation Pathway in Many-Particle $LiFePO_4$ Electrode Revealed by Nanoscale State-of-Charge Mapping. *Nano Lett.* **2013**, *13*, 866–872.
20. Cabana, J.; Shirakawa, J.; Chen, G.; Richardson, T. J.; Grey, C. P. MAS NMR Study of the Metastable Solid Solutions Found in the $LiFePO_4$/$FePO_4$ System. *Chem. Mater.* **2010**, *22*, 1249–1262.
21. Delacourt, C.; Poizot, P.; Tarascon, J.-M.; Masquelier, C. The Existence of a Temperature-Driven Solid Solution in Li_xFePO_4 for $0 < x < 1$. *Nat. Mater.* **2005**, *4*, 254–260.
22. Sharma, N.; Guo, X.; Du, G.; Guo, Z.; Wang, J.-Z.; Wang, Z.; Peterson, V. K. Direct Evidence of Concurrent Solid-Solution and Two-Phase Reactions and the Non-Equilibrium Structural Evolution of $LiFePO_4$. *J. Am. Chem. Soc.* **2012**, *134*, 7867–7873.
23. Dedryvère, R.; Maccario, M.; Croguennec, L.; Le Cras, F.; Delmas, C.; Gonbeau, D. X-Ray Photoelectron Spectroscopy Investigations of Carbon-Coated Li_xFePO_4 Materials. *Chem. Mater.* **2008**, *20*, 7164–7170.
24. Castro, L.; Dedryvère, R.; Ledeuil, J.-B.; Bréger, J.; Tessier, C.; Gonbeau, D. Aging Mechanisms of $LiFePO_4$ // Graphite Cells Studied by XPS: Redox Reaction and Electrode/Electrolyte Interfaces. *J. Electrochem. Soc.* **2012**, *159*, A357–A363.
25. Liu, J.; Kunz, M.; Chen, K.; Tamura, N.; Richardson, T. J. Visualization of Charge Distribution in a Lithium Battery Electrode. *J. Phys. Chem. Lett.* **2010**, *1*, 2120–2123.
26. Ouvrard, G.; Zerrouki, M.; Soudan, P.; Lestriez, B.; Masquelier, C.; Morcrette, M.; Hamelet, S.; Belin, S.; Flank, A. M.; Baudelet, F. Heterogeneous Behaviour of the Lithium Battery Composite Electrode $LiFePO_4$. *J. Power Sources* **2013**, *229*, 16–21.
27. Allen, J. L.; Jow, T. R.; Wolfenstine, J. Kinetic Study of the Electrochemical $FePO_4$ to $LiFePO_4$ Phase Transition. *Chem. Mater.* **2007**, *19*, 2108–2111.
28. Oyama, G.; Yamada, Y.; Natsui, R.; Nishimura, S.; Yamada, A. Kinetics of Nucleation and Growth in Two-Phase Electrochemical Reaction of Li_xFePO_4. *J. Phys. Chem. C* **2012**, *116*, 7306–7311.
29. Orikasa, Y.; Maeda, T.; Koyama, Y.; Murayama, H.; Fukuda, K.; Tanida, H.; Arai, H.; Matsubara, E.; Uchimoto, Y.; Ogumi, Z. Transient Phase Change in Two Phase Reaction between $LiFePO_4$ and $FePO_4$ under Battery Operation. *Chem. Mater.* **2013**, *25*, 1032–1039.
30. Brodusch, N.; Demers, H.; Gauvin, R. Nanometres-Resolution Kikuchi Patterns from Materials Science Specimens with Transmission Electron Forward Scatter Diffraction in the Scanning Electron Microscope. *J. Microsc.* **2013**, *250*, 1–14.
31. Trimby, P. W. Orientation Mapping of Nanostructured Materials Using Transmission Kikuchi Diffraction in the Scanning Electron Microscope. *Ultramicroscopy* **2012**, *120*, 16–24.
32. Keller, R. R.; Geiss, R. H. Transmission EBSD from 10 nm Domains in a Scanning Electron Microscope. *J. Microsc.* **2012**, *245*, 245–251.
33. Chang, H.-H.; Chang, C.-C.; Wu, H.-C.; Yang, M.-H.; Sheu, H.-S.; Wu, N.-L. Study on Dynamics of Structural Transformation during Charge/Discharge of $LiFePO_4$ Cathode. *Electrochem. Commun.* **2008**, *10*, 335–339.
34. Shin, H. C.; Chung, K. Y.; Min, W. S.; Byun, D. J.; Jang, H.; Cho, B. W. Asymmetry between Charge and Discharge during High Rate Cycling in $LiFePO_4$ – *In Situ* X-ray Diffraction Study. *Electrochem. Commun.* **2008**, *10*, 536–540.
35. Srinivasan, V.; Newman, J. Existence of Path-Dependence in the $LiFePO_4$ Electrode. *Electrochem. Solid-State Lett.* **2006**, *9*, A110–A114.
36. Peled, E. The Electrochemical Behavior of Alkali and Alkaline Earth Metals in Nonaqueous Battery Systems—The Solid Electrolyte Interphase Model. *J. Electrochem. Soc.* **1979**, *126*, 2047–2051.
37. Dey, A. N.; Sullivan, B. P. The Electrochemical Decomposition of Propylene Carbonate on Graphite. *J. Electrochem. Soc.* **1970**, *117*, 222–224.
38. Aurbach, D.; Markovsky, B.; Weissman, I.; Levi, E.; Ein-Eli, Y. On the Correlation between Surface Chemistry and Performance of Graphite Negative Electrodes for Li Ion Batteries. *Electrochim. Acta* **1999**, *45*, 67–86.
39. Aurbach, D.; Zinigrad, E.; Cohen, Y.; Teller, H. A Short Review of Failure Mechanisms of Lithium Metal and Lithiated Graphite Anodes in Liquid Electrolyte Solutions. *Solid State Ionics* **2002**, *148*, 405–416.
40. Winter, M.; Besenhard, J. O.; Spahr, M. E.; Novák, P. Insertion Electrode Materials for Rechargeable Lithium Batteries. *Adv. Mater.* **1998**, *10*, 725–763.
41. Fongy, C.; Gaillot, A.-C.; Jouanneau, S.; Guyomard, D.; Lestriez, B. Ionic vs Electronic Power Limitations and Analysis of the Fraction of Wired Grains in $LiFePO_4$ Composite Electrodes. *J. Electrochem. Soc.* **2010**, *157*, A885–A891.